Journal of Alloys and Compounds 509 (2011) 1544–1549

Contents lists available at ScienceDirect

Journal of Alloys and Compounds

journal homepage: www.elsevier.com/locate/jallcom

The effect of Ag concentration on the structural, electrical and thermal transport behavior of Pb:Te:Ag:Se mixtures and improvement of thermoelectric performance via Cu doping

J. Capps[a], B. Ma[a], T. Drye[b], C. Nucklos[a], S. Lindsey[a], D. Rhodes[a], Q. Zhang[a], K. Modic[c], S. Cawthorne[a], F. Drymiotis[a,*]

[a] Clemson University, Clemson, SC 29634, USA
[b] University of Maryland, College Park, MD 20742, USA
[c] University of Texas, Austin, TX 78712, USA

ARTICLE INFO

Article history:
Received 3 April 2010
Received in revised form 26 October 2010
Accepted 29 October 2010
Available online 9 November 2010

Keywords:
Thermoelectric materials
Composites
Phase transition
ZT

ABSTRACT

Pb, Te, Ag and Se, when reacted in a 1:1:*x*:1 (*x* = 1.9, 2.0, 2.01) molar ratio, form a two phase composite which consists of a phase which crystallizes in the fcc cubic PbSe structure and a phase that crystallizes in the Ag_2Te structure. In this article, we demonstrate that by varying the Ag concentration, we can manipulate which variant of the Ag_2Te structure stabilizes at room temperature (monoclinic α-Ag_2Te or cubic β-$Ag_{1.9}Te$) and can consequently manipulate the electrical and thermal transport behavior of the composite and hence the thermoelectric performance. Additionally, we show that Cu-doping results in an overall improvement in thermoelectric performance. Our results suggest that formation of composites is a viable path for achieving a phonon-glass-electron-crystal (PGEC) alloy.

1. Introduction

Sustainable energy research is currently on the forefront of scientific exploration thus a major effort is devoted to the development of new energy conservation and production techniques. Thermoelectric materials can play a significant part both in energy conservation and energy production, since they can convert wasted heat to useful electrical energy [1–4]. For power generation applications, the dimensionless figure of merit (ZT) should be maximized at or above temperatures of 400 °C. The figure of merit is given by $\alpha^2\sigma T/\kappa$, where α is the thermopower or Seebeck coefficient, σ is the electrical conductivity, and κ is the thermal conductivity. Maximizing thermoelectric performance implies minimizing the thermal conductivity and maximizing the electrical conductivity and thermopower. Unfortunately these three parameters are not independent. For example, metallic electronic conductivity will lead to low thermopower, and high thermal conductivity because of large electronic heat conduction. Semimetals and narrow-gap semiconductors tend to give the best thermoelectric performance because of their low-carrier concentration which limits electronic heat conduction, and their relatively high thermopower. Still, optimization of the parameters is required in order to achieve the maximum thermoelectric performance for a particular alloy. Optimization can be achieved through doping or mechanical processing or both.

Our approach to design a highly efficient thermoelectric material is to begin with an alloy that has inherently low thermal conductivity. Such a scenario can be realized for example in single phase compounds which have large and complex unit cells [5], or in complex multi-phase structures in which phase competition and disorder lead to low thermal conductivity. We opted to follow the latter approach. If the electrical conductivity remains favorable then the structure will offer a good starting point for optimization. The goal is the formation of a PGEC [5,6] i.e. an alloy which has the electronic properties of a crystalline system and the thermal transport behavior of a glass. A typical approach is to form mixtures of known thermoelectric materials at various molar ratios which may lead to the formation of multi-phase composites or single-phase highly disordered compounds (depending on the relative molar ratios). This approach has yielded very interesting results with the most notable case being the alloy $(PbTe)_m(AgSbTe_2)$, in which a dimensional figure of merit ZT >1.8 was measured [7] for $m = 18$. In that particular case, a reduction in total thermal conductivity (when compared to stoichiometric PbTe) was induced by enhanced phonon scattering due to the presence of nanoscale inhomogeneities [8–13]. However, reproducibility of the original results has proven extremely difficult.

* Corresponding author. Tel.: +1 864 656 5317.
E-mail address: fdrymio@clemson.edu (F. Drymiotis).

0925-8388/$ – see front matter © 2010 Elsevier B.V. All rights reserved.
doi:10.1016/j.jallcom.2010.10.187

We chose to react Pb:Te:Ag:Se in a 1:1:x:1 (x = 1.9, 2.0, 2.01) molar ratio in order to monitor the effects of phase competition between the cubic PbSe and the monoclinic α-Ag_2Te. In a previous article [14] we showed that reacting Pb:Te:Ag:Se in a 1:1:1.9:1 molar ratio, gives rise to a predominantly single phase alloy, which crystallizes in the PbSe cF8 fcc structure, and has good thermoelectric performance. Further investigation of the structure, using EDX, revealed the coexistence of two-phases. In this article, we demonstrate that by varying the Ag concentration we can control the phase formed by the Ag_2Te, and by doping Cu into the structure, we can induce changes in the thermal and electrical transport behavior which allows us to optimize thermoelectric performance.

2. Experimental

The Pb:Te:Ag:Se (1:1:x:1 x = 1.9, 2.0, 2.01) and the Pb:Te:Ag:Cu:Se (1:1:x:y:1 x = 1.85, 1.8 y = 0.05, 0.1) samples were grown according to the method described in Ref. [14]. The X-ray diffraction data was obtained using a commercial Rigaku® diffractometer and the SEM and EDX analysis were performed using the Hitachi S3400-N and SU6600 SEMs. The high-temperature resistivity and thermopower data were obtained using the ULVAC-ZEM2® measuring system. The high-temperature thermal-conductivity values were deduced from the thermal diffusivity values obtained using the Netzsch LFA 457® laser flash apparatus using the relation $\kappa = \alpha d C_P$, with α being the measured value of the thermal diffusivity, d the density and C_P the heat capacity at constant pressure. The value of d used in the calculations was the measured density at room temperature, and the value of C_P was taken to be the value of the DuLong Petit limit. The calorimetry data were taken using the Netzsch 200 F3® DSC. The density of all samples was approximately 8 g/cm^3.

3. Results and discussion

The Ag–Te phase diagram is fairly complicated [15] in the region corresponding to Ag_2Te. In particular, Ag_2Te undergoes 2 structural phase transitions prior to melting at 960 °C. The α-Ag_2Te ↔ β-Ag_2Te phase transition, corresponding to monoclinic to cubic (fcc) transformation, takes place at 145 °C, and the β-Ag_2Te ↔ γ-Ag_2Te phase transition, corresponding to cubic (fcc) to cubic (bcc) transformation, takes place at 802 °C. If the system contains extra Te, the β ↔ γ transition takes place at 689 °C. In addition, a stoichiometric phase $Ag_{1.9}Te$ can also be stabilized, and also undergoes a series of phase transitions before it transforms to β-Ag_2Te + L at 460 °C (β-$Ag_{1.9}Te$ ↔ β-Ag_2Te + L). Specifically, the transition α-$Ag_{1.9}Te$ ↔ α-Ag_2Te + α-Ag_5Te_3 takes place at 120 °C, and the α-$Ag_{1.9}Te$ ↔ β-$Ag_{1.9}Te$ transition takes place at 178 °C.

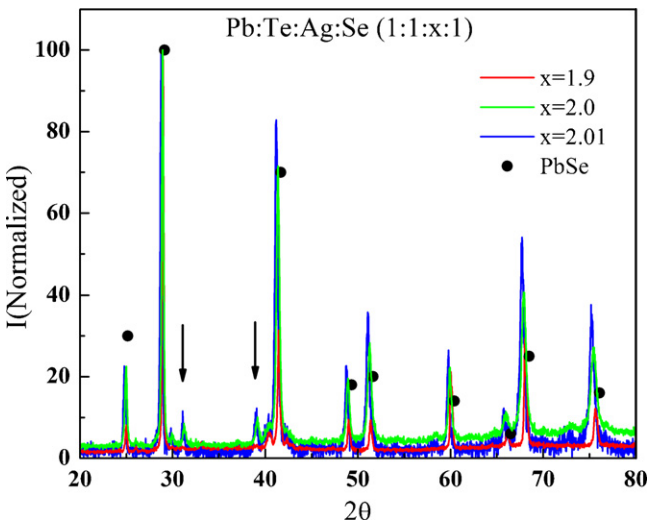

Fig. 1. Room temperature X-ray diffraction data for Pb:Te:Ag:Se (1:1:x:1), x = 1.9, 2.0 and 2.01. Peaks corresponding to α-Ag_2Te can be seen in the case of the x = 2.0 and 2.01 sample. The black dots correspond to the location of the peaks of stoichiometric PbSe. The arrows show the location of the strongest peaks of the monoclinic α-Ag_2Te phase.

According to the X-ray diffraction data, reacting Pb:Te:Ag:Se in a 1:1:1.9:1 molar ratio gives rise to what appears to be a single phase alloy that crystallizes in the face-centered-cubic (fcc) PbSe structure. However, energy dispersive X-ray analysis (EDX), reveals the existence of 2 phases with distinct stoichiometry: a phase with the stoichiometry PbSe (1:1) and a phase with the stoichiometry Ag_2Te (2:1); hence the formed alloy is a two phase composite. The X-ray diffraction data is shown in Fig. 1 and the elemental mapping of an alloy with a nominal composition $PbTeAg_{1.9}Te$ is

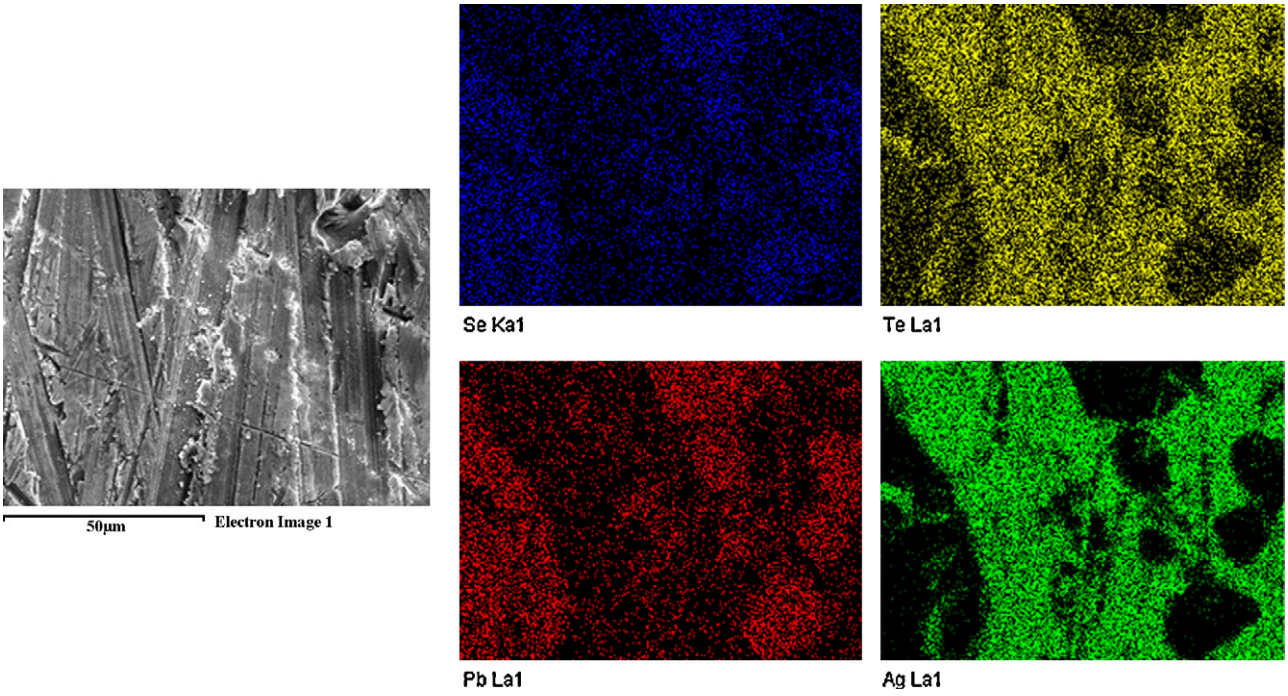

Fig. 2. Elemental mapping for Pb:Te:Ag:Se (1:1:x:1, x = 1.9). The SEM image of the composite is shown in the upper left corner. Elemental mapping shows the preference of Pb to react with Se and of Ag to react with the Te.

shown in Fig. 2. The elemental mapping clearly shows the Pb–Se and Ag–Te grouping which confirms the preference of Se to react with the Pb and the preference of Te to react with the Ag. The crystal structure of the Ag_2Te phase remains in question, but according to the X-ray diffraction data, in the case of $x = 1.9$, it appears that the Ag_2Te phase crystallizes predominantly in its high temperature cubic variant (β-Ag_2Te or β-$Ag_{1.9}Te$). Small amounts of the monoclinic α-Ag_2Te are also evident in the X-ray data. The presence of the monoclinic α-Ag_2Te phase becomes more evident as we increase the Ag concentration. Particularly, in the $x = 2.0$ and $x = 2.01$ samples, the strongest peaks corresponding to the monoclinic α-Ag_2Te phase can be observed at $2\theta \sim 31^\circ$ and $2\theta \sim 38^\circ$ (Fig. 2).

Similarly, in the case of the Cu-doped samples ($PbTeAg_{1.85}Cu_{.05}Se$ and $PbTeAg_{1.80}Cu_{.1}Se$), the X-ray diffraction data (Fig. 3) also suggests that the resulting alloy is single phase, and that it crystallizes in an fcc structure. However, in the case of the $PbTeAg_{1.8}Cu_{.1}Se$ sample, there is an increase in the lattice parameter and the appearance of impurity peaks. The origin of the impurity peaks is most likely the formation of the β-Ag_5Te_3 phase, whose presence is confirmed in the differential scanning calorimeter (DSC) measurements. EDX analysis (Fig. 4) for the $x = 1.8$ $y = 0.1$ sample shows clearly the presence of 2 distinct phases which appear to occupy similar volume fractions. The two distinct phases have been identified as PbSe and Ag_2Te. According to the elemental map, the Cu appears to be distributed throughout the material, but according to localized EDX measurements, the Cu concentration in the Ag_2Te regions is slightly higher than the Cu-concentration in the PbSe regions. Localized EDX measurements reveal the following compositions: (a) PbSe phase, Pb 48.46 at.%, Se 46.90 at.%, Te 4.23 at.%, Cu 0.4 at.% and (b) Ag_2Te phase, Ag 64.10 at.%, Te 29.95 at.%, Se 3.77 at.%, Cu 2.18 at.%. The variations in the atomic percentages are of the order of 1.5%. Regardless, the X-ray diffraction data in conjunction with the EDX measurements, confirms that the Ag_2Te indeed stabilizes in its high-temperature cubic variant when the Ag concentration is reduced.

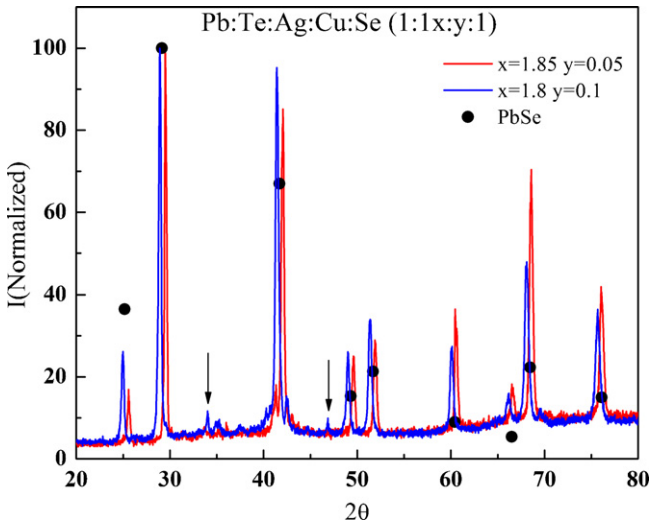

Fig. 3. Room temperature X-ray diffraction data for Pb:Te:Ag:Cu:Se (1:1:*x*:*y*:1), $x = 1.85$ $y = 0.05$ and $x = 1.8$ $y = 0.1$. The dominant structure is fcc and an increase in the lattice parameter occurs in the $x = 1.8$ $y = 0.1$ sample. The arrows show the location of impurity peaks, most probably corresponding to the presence of Ag_5Te_3. The black dots correspond to the location of the peaks of stoichiometric PbSe.

In order to confirm that removing Ag from the structure results in the stabilization of the high temperature cubic structure, a differential scanning calorimeter (DSC) was utilized in order to study the temperature evolution of the structure as a function of Ag concentration ($x = 1.9$, 2.0 and 2.01 ($y = 0$)). The relevant data is shown in Fig. 5. For $x = 2.0$ and $x = 2.01$, a transition can be clearly seen around $T \sim 140\,^\circ$C. The calculated onset of the transition is $T = 130\,^\circ$C and it corresponds to the α-$Ag_2Te \leftrightarrow$ β-Ag_2Te structural phase transition. In the case of the $x = 1.9$ $y = 0$ samples, the transition at $T = 130\,^\circ$C is suppressed, which implies that only traces of the monoclinic α-Ag_2Te phase are present in the sample. A transition though appears

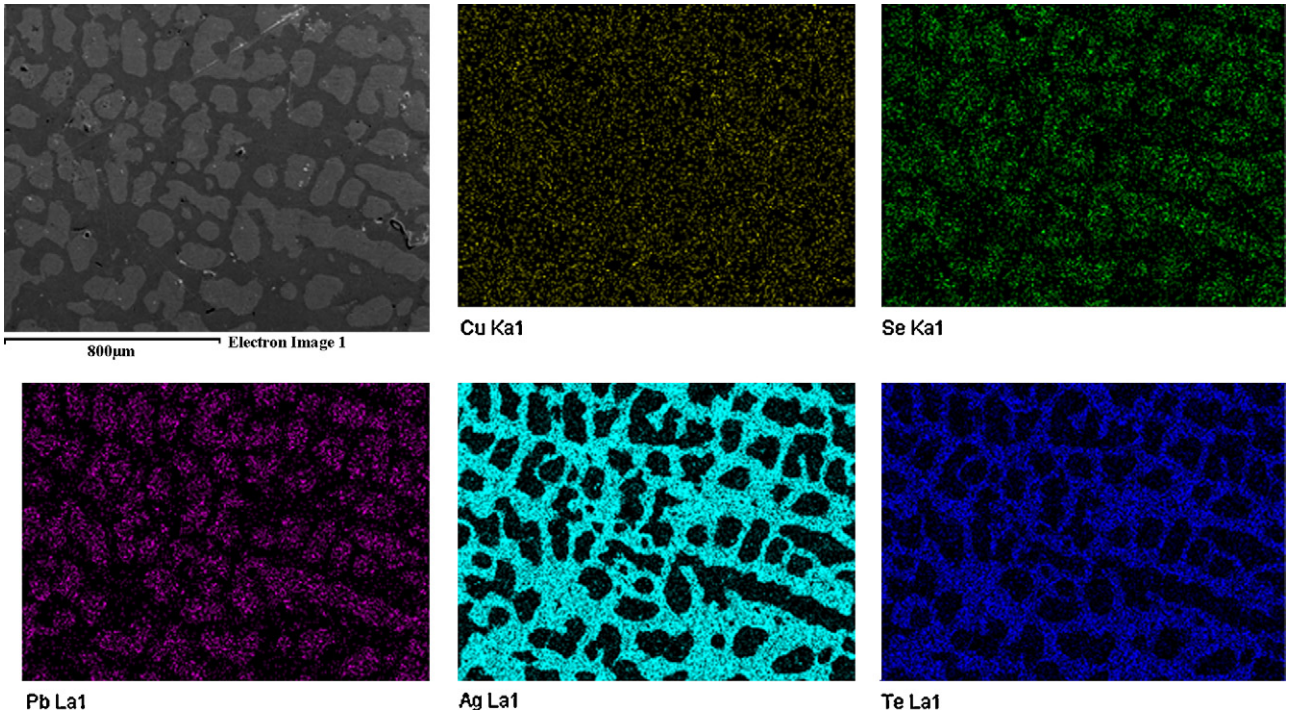

Fig. 4. Elemental mapping for a polished Pb:Te:Ag:Cu:Se (1:1:*x*:*y*:1, $x = 1.8$ $y = 0.1$) sample. The SEM image of the composite is shown in the upper left corner. Two distinct phases can be observed which have been identified as PbSe (light gray) and Ag_2Te (dark gray). The element distribution confirms the Pb–Se, Ag–Te grouping. Cu appears to be uniformly distributed throughout the sample, though according to local EDX measurements it has a preference for the Ag_2Te phase.

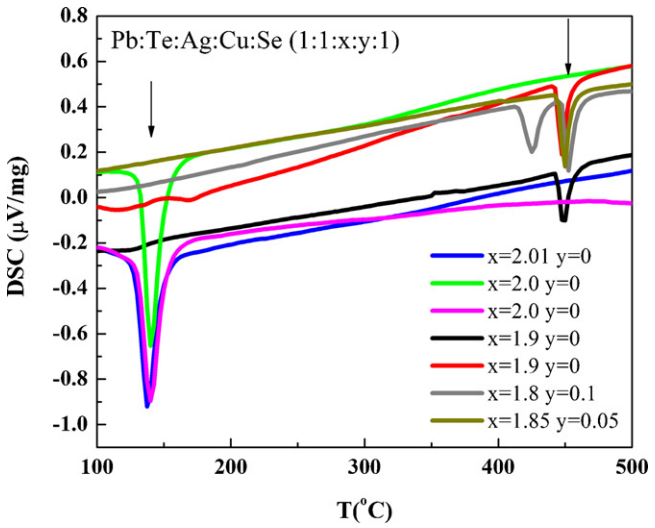

Fig. 5. Differential scanning calorimeter data for Pb:Te:Ag:Cu:Se (1:1:*x*:*y*:1). The transition at 130 °C, seen only in the $x = 2.0$ $y = 0$ and $x = 2.01$ $y = 0$ samples, corresponds to the α-Ag_2Te ↔ β-Ag_2Te phase transition. The transition at 443 °C, seen only in the case of the $x = 1.9$ $y = 0$ samples corresponds to the β-$Ag_{1.9}Te$ ↔ β-Ag_2Te + L phase transition. Suppression of the α-Ag_2Te ↔ β-Ag_2Te transition is also observed in the case of the $x = 1.85$ $y = 0.05$ and $x = 1.8$ $y = 0.1$ samples. However, in the case of the $x = 1.8$ $y = 0.1$ sample, a transition appears at $T \sim 420$ °C, which corresponds to β-Ag_5Te_3 ↔ β-$Ag_{1.9}Te$ + L.

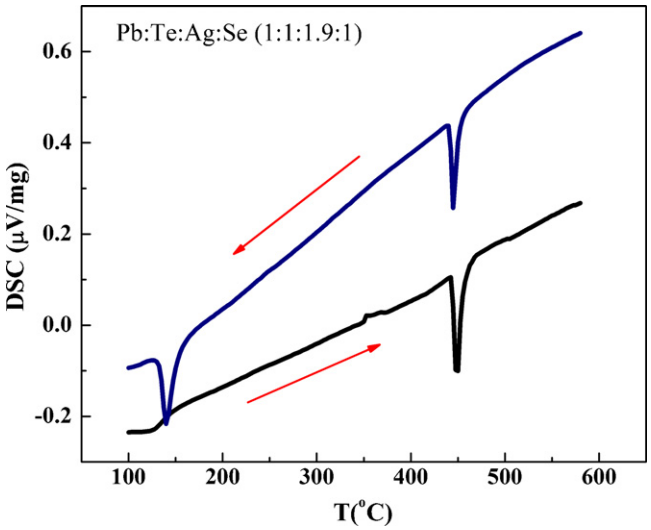

Fig. 6. Differential scanning calorimeter data for the $x = 1.9$ $y = 0$ sample. Heating the sample above the β-$Ag_{1.9}Te$ ↔ β-Ag_2Te + L phase transition (black line) leads to the formation of β-Ag_2Te which persists as the temperature is lowered below β-$Ag_{1.9}Te$ ↔ β-Ag_2Te + L the transition. Consequently upon cooling, both α-Ag_2Te ↔ β-Ag_2Te and β-$Ag_{1.9}Te$ ↔ β-Ag_2Te + L transitions are present (blue line) (For interpretation of the references to color in this figure legend, the reader is referred to the web version of the article).

at $T \sim 450$ °C (calculated onset at $T = 443$ °C) which corresponds to the β-$Ag_{1.9}Te$ ↔ β-Ag_2Te + L structural phase transition. Removing Ag from the structure ($x = 2.0 \rightarrow x = 1.9$) leads to the stabilization of the high temperature cubic β-$Ag_{1.9}Te$ phase at room temperature. In the case of the Cu-doped samples ($x = 1.8$ $y = 0.1$, $x = 1.85$ $y = 0.05$), the α-Ag_2Te ↔ β-Ag_2Te structural phase transition has been eliminated in but in the case of the $x = 1.8$ $y = 0.1$ sample another peak appears at a temperature $T \sim 420$ °C (calculated onset at $T = 415$ °C), which corresponds to the β-Ag_5Te_3 ↔ β-$Ag_{1.9}Te$ + L transition. The appearance of the Ag_5Te_3 is reasonable when one considers that the Ag concentration has been reduced by 10% (Ag_2 to $Ag_{1.8}$).

Additionally, according to the DSC data shown in Fig. 5, heating the $x = 1.9$ samples past the β-$Ag_{1.9}Te$ ↔ β-Ag_2Te + L structural phase transition leads to the formation of β-Ag_2Te, which remains present after cooling through the transition and leads to the deterioration of the thermoelectric performance. Its existence is confirmed by the appearance of the transition at $T = 130$ °C, in addition to the transition at $T = 443$ °C, on cooling (Fig. 6).

The electrical and thermal transport behavior of these composites is strongly affected by the Ag and Cu concentration. Distinct differences can be seen in the resistivity, thermopower and thermal conductivity behavior. The resistivity (Fig. 7) of the $x = 2$ $y = 0$ and $x = 2.01$ $y = 0$ samples increases with increasing temperature, and can be described as metallic in the temperature region $50\,°C \leq T \leq 400\,°C$. The resistivity value at $T = 50$ °C for both the $x = 2$ and $x = 2.01$ samples is $\rho = 1.3 \times 10^{-5}\ \Omega\,m$. Only a small feature corresponding to the α → β structural phase transition can be seen. The resistivity for the $x = 1.9$ $y = 0$ samples on the other hand, shows activated behavior. Its value at $T = 50$ °C is $\rho = 5.0 \times 10^{-4}\ \Omega\,m$, which is considerably larger than the resistivity of the $x = 2$ and $x = 2.01$ samples. In addition, there is no feature at $T = 130$ °C; this is presumably due to the very small amount of α-Ag_2Te present in the sample. The upturn in the resistivity of the $x = 1.9$ $y = 0$ samples at $T \sim 300$ °C, is due to minority carrier contribution. In the case of the Cu-doped samples, the resistivity also shows activated behavior, and their resistivity values are comparable to those of the $x = 1.9$ $y = 0$ samples. However, the resistivity of the Cu-doped samples is lower in the temperature region between 300 °C and

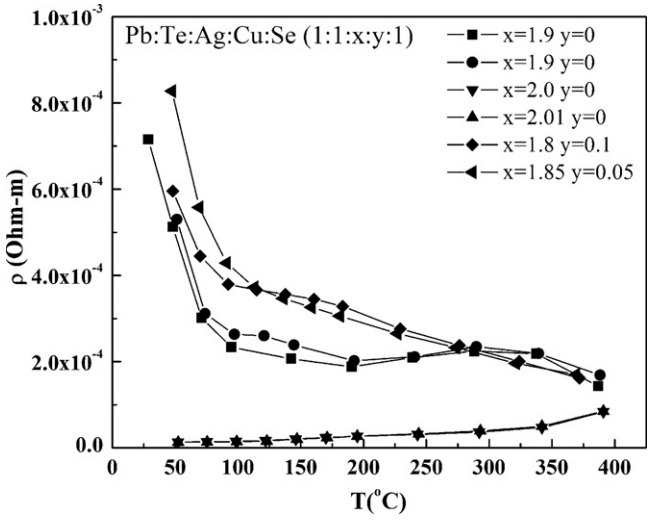

Fig. 7. High temperature resistivity data for the Pb:Te:Ag:Cu:Se (1:1:*x*:*y*:1) samples. Reducing the Ag concentration causes the resistivity to increase considerably. The upturn at $T = 300$ °C for the $x = 1.9$ $y = 0$ sample is due to minority carrier contribution. The $x = 2.0$ $y = 0$ and $x = 2.01$ $y = 0$ samples show metallic behavior. The reduced-Ag concentration and Cu-doped samples show activated behavior.

375 °C ($1.8 \times 10^{-4}\ \Omega\,m$ versus $2.1 \times 10^{-4}\ \Omega\,m$ at $T = 350$ °C) because of the absence of minority carrier contribution. The reduction in resistivity in that temperature region contributes to the improved thermoelectric efficiency.

The thermopower, shown in Fig. 8, changes dramatically as Ag is removed from the structure. In the case of the $x = 2.0$ and $x = 2.01$ samples, the thermopower is small and negative, indicating n-type behavior. Both samples display identical temperature dependence, albeit a slight decrease in the magnitude of the thermopower in the case of the $x = 2.01$ sample. This suggests that excess Ag makes the sample more metallic. For both $x = 2.0$ and $x = 2.01$ concentrations, there is a clear feature at $T = 130$ °C corresponding to the α-Ag_2Te ↔ β-Ag_2Te structural phase transition. The thermopower below the transition appears to be weakly tem-

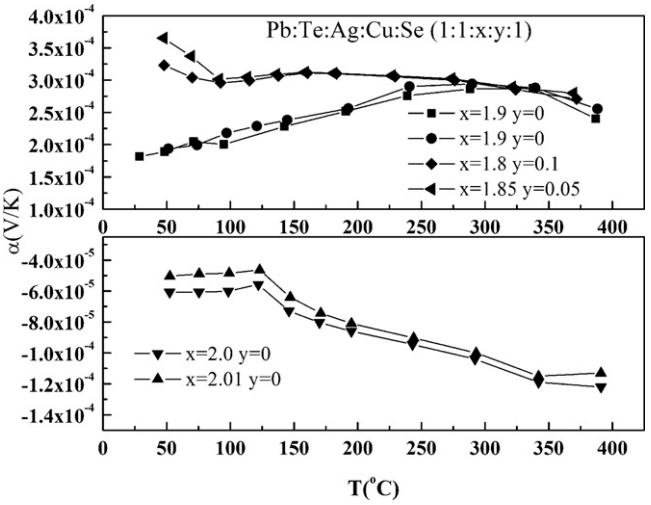

Fig. 8. High temperature thermopower data for the Pb:Te:Ag:Cu:Se (1:1:*x*:*y*:1) samples. Reducing the Ag concentration changes the thermopower from n-type to p-type. The maximum in the thermopower observed at $T = 300\,^{\circ}C$ for the $x = 1.9$ $y = 0$ sample is due to minority carrier contribution, in agreement with the resistivity data. The thermopower values for the Cu-doped samples are higher than the $x = 1.9$ $y = 0$ sample for $T < 300\,^{\circ}C$ but for $T > 300\,^{\circ}C$ the values are identical.

perature dependent, while above the transition it becomes more negative with increasing temperature. The absolute values of the thermopower for both $x = 2.0$ and $x = 2.01$ samples, in the temperature range $50\,^{\circ}C \leq T \leq 400\,^{\circ}C$, are smaller than the corresponding values of pure Ag_2Te [16–19] but this is most probably due to the presence of impurities. The sign of the thermopower though is in agreement. In the case of the $x = 1.9$ samples, the sign of the thermopower changes to positive, indicating p-type behavior. In addition, the magnitude of the thermopower increases considerably when compared to the $x = 2.0$ and 2.01 samples. The decrease in thermopower at $T \sim 300\,^{\circ}C$ is due to minority carrier contribution and it coincides with the feature in the resistivity. There is no noticeable feature at $T = 130\,^{\circ}C$ which implies that the α-Ag_2Te is suppressed, in agreement with the DSC data. In the case of the Cu-doped samples, there is a notable increase in the thermopower at lower temperatures, but at high temperatures the thermopower values are similar to the ones obtained in the $x = 1.9$ $y = 0$ samples.

An n → p change was observed in an $Ag_{1.9}Te$ sample that we synthesized, with the n → p transition coinciding with the monoclinic to cubic phase transition (Fig. 9). The resistivity shows a metal to insulator transition at that temperature as well. The magnitude of the thermopower in that sample, at high temperature, is comparable to the magnitude observed in these composites, which offers further proof that the Ag_2Te stabilizes in a cubic phase. The thermopower of the stoichiometric Ag_2Te remains negative through the transition [19] which implies that in the $Ag_{1.9}Te$ sample, the composition of the cubic phase is β-$Ag_{1.9}Te$ and not β-Ag_2Te and that the p-type behavior in the composites is associated with the reduction in Ag concentration.

The thermal conductivity data are shown in Fig. 10. In the case of the $x = 2.0$ and $x = 2.01$ samples, the total thermal conductivity at $T = 50\,^{\circ}C$ is approximately $\kappa_T \sim 1\,W/m\,K$ but it does vary with Ag concentration (due to variations in nominal versus actual Ag concentration for $x = 2$ and $x = 2.01$). The thermal conductivity decreases with increasing temperature as the α-Ag_2Te ↔ β-Ag_2Te transition temperature is approached. Both $x = 2.0$ and $x = 2.01$ samples display approximately a 30% reduction in the thermal conductivity as the samples go through the transition. Above the structural phase transition, the total thermal conductivity remains relatively temperature independent. The data suggests that the presence of α-Ag_2Te dictates the behavior of the thermal conductivity below the transition. On the other hand, a large reduction in the total thermal conductivity is observed for the $x = 1.9$ samples throughout the temperature range, and the feature at $T = 130\,^{\circ}C$ has been suppressed, indicating that the amount of α-Ag_2Te in the sample has been substantially reduced (data points taken at closer temperature intervals in the temperature region of the transition show a weak feature at the transition temperature which is consistent with the suppression of the α-Ag_2Te phase).

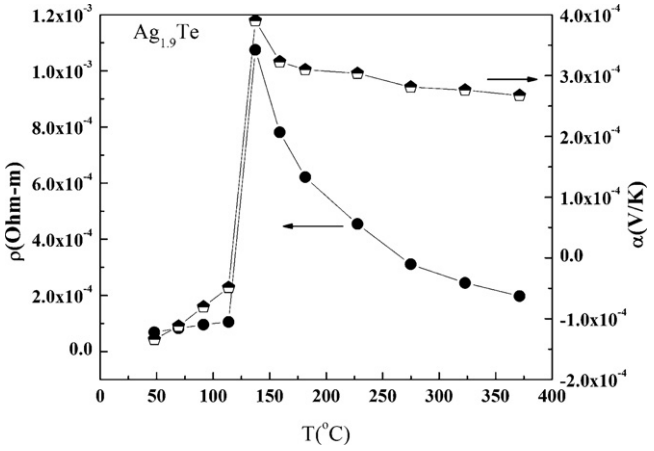

Fig. 9. Resistivity (solid circles-left axis) and thermopower (black/white pentagons-right axis) of $Ag_{1.9}Te$. The n → p change coincides with the monoclinic to cubic structural phase transition. The resistivity shows metal to insulator transition as the sample goes through the transition.

According to the Wiedemann–Franz relation (with $L \sim 2.0 \times 10^{-8}\,W\,\Omega\,K^{-2}$), in the case of the $x = 1.9$ $y = 0$ samples, for $\kappa_T = 0.57\,W/m\,K$ and $\rho = 1.7 \times 10^{-4}\,\Omega\,m$, the electronic and lattice contributions to the thermal conductivity at $T = 390\,^{\circ}C$ are 0.08 W/m K and 0.49 W/m K respectively; whereas in the case of the $x = 2.0$ samples, for $\kappa_T = 0.77\,W/m\,K$ (average value) and $\rho = 8.5 \times 10^{-5}\,\Omega\,m$, the electronic and lattice contributions to the thermal conductivity at $T = 390\,^{\circ}C$ are 0.15 W/m K and 0.62 W/m K respectively. Hence, reducing the Ag concentration enhances phonon scattering.

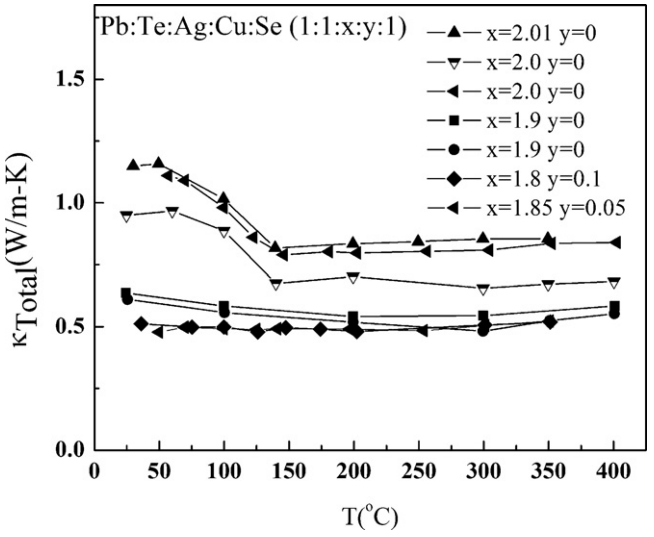

Fig. 10. High temperature thermal conductivity data for the Pb:Te:Ag:Cu:Se (1:1:*x*:*y*:1) samples. The transition at 130 °C, seen only in the $x = 2.0$ $y = 0$ and $x = 2.01$ $y = 0$ samples, corresponds to the α-Ag_2Te ↔ β-Ag_2Te phase transition. The transition is strongly suppressed in the $x = 1.9$ $y = 0$ samples which also show a reduction in total thermal conductivity. A further reduction, albeit slight, is observed in the Cu doped ($x = 1.85$ $y = 0.05$, $x = 1.8$ $y = 0.1$) samples.

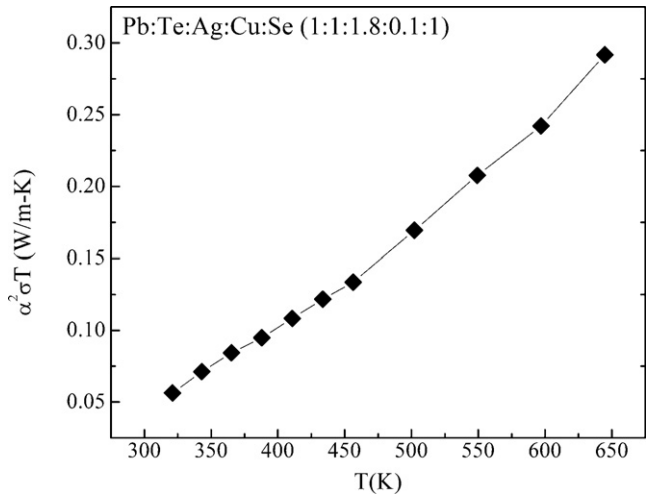

Fig. 11. Power factor, $\alpha^2\sigma T$, as a function of temperature for $PbTeAg_{1.8}Cu_{0.1}Se$.

A further reduction in the total thermal conductivity is observed in the case of the Cu-doped samples; the reduction is slight. In particular, in the case of the $x = 1.8$ $y = 0.1$ sample, the total thermal conductivity at $T = 350\,^{\circ}C$ is approximately $\kappa_T = 0.52$ W/m K, which corresponds to a ~5% reduction when compared to the thermal conductivity of one of the $x = 1.9$ $y = 0$ samples at the same temperature ($\kappa_T = 0.55$ W/m K). However, another $x = 1.9$ $y = 0$ sample displayed a similar thermal conductivity value at the same temperature. This suggests that the decrease in the thermal conductivity can be attributed to both Cu addition and reduction in Ag concentration. There is a distinct difference however in the temperature dependence of the thermal conductivity between the $x = 1.9$ $y = 0$ samples and the Cu doped samples. In the temperature region between 50 °C and 200 °C the thermal conductivity of the $x = 1.9$ $y = 0$ samples decreases with increasing temperature, while in the Cu-doped samples it is flat, which suggests that the monoclinic phase has been eliminated, in agreement with the DSC data.

The calculated ZT in the case of the $x = 1.9$ $y = 0$ samples was $ZT = 0.45$ at $T = 390\,^{\circ}C$ whereas in the case of the $x = 1.8$ $y = 0.1$ sample, $ZT = 0.54$ at $T = 350\,^{\circ}C$, which corresponds to a 20% increase. The power factor, defined as $\alpha^2\sigma T$ (where $\sigma = 1/\rho$), for the $x = 1.8$ $y = 0.1$ sample is shown in Fig. 11. ZT values can be obtained by diving the power factor with the thermal conductivity value at a specific temperature ($ZT = \alpha^2\sigma T/\kappa$). The linear increase of the power factor as a function of temperature is promising but unfortunately our temperature range is limited due to the oncoming structural phase transition, which deteriorates the samples and the thermoelectric performance. Nonetheless, we have been able to improve the thermoelectric performance of these composites via Cu-doping.

4. Conclusions

The phase separation in Pb:Te:Ag:Se mixtures allows for substantial manipulation of the lattice. We have shown that slight variations in Ag concentration lead to substantial changes in the electrical and thermal transport through phase control. The maximum thermoelectric performance obtained in the non-Cu-doped composites is $ZT \sim 0.45$ [14] and we have shown in this article that $ZT \sim 0.54$ can be achieved via Cu doping. The thermoelectric efficiency is too low to be competitive, but higher ZT values have been obtained in $AgSbTe_2$:Ag_2Se composites [20]. However, further lattice manipulation and processing may result in higher ZT values. We are currently investigating the effect of other dopants and additional reduction in Ag concentration, in an effort to further improve thermoelectric performance. We are also investigating the effects of magnetic impurities. Regardless, our work suggests that formation of multi-component composites, formed by reacting certain elements in specific molar combinations, is a viable approach to developing a PGEC.

Acknowledgements

We would like to thank NSF-DMR-0905322 for support of this project. We would also like to thank Dr. Terry Tritt for allowing us access to his measurement apparatus.

References

[1] L.E. Bell, Science 321 (2008) 1457.
[2] G.S. Nolas, Thermoelectric materials 2003–research and applications: symposium held December 1–3, 2003, Boston, Massachusetts, U.S.A (Materials Research Society, Warrendale, Pa., 2004), pp. xiv.
[3] G.J. Snyder, E.S. Toberer, Nature Materials 7 (2008) 105.
[4] T.M. Tritt, Thermoelectric materials 2000–the next generation materials for small-scale refrigeration and power generation applications: symposium held April 24–27, 2000, San Francisco, California, U.S.A (Materials Research Society, Warrendale, Pa., 2001), p. 1 v.(various pagings).
[5] G.S. Nolas, J. Sharp, H.J. Goldsmid, Thermoelectrics: Basic Principles And New Materials Developments, Springer, Berlin; New York, 2001, pp. viii.
[6] G.A. Slack, V.G. Tsoukala, Journal of Applied Physics 76 (1994) 1665.
[7] K.F. Hsu, S. Loo, F. Guo, W. Chen, J.S. Dyck, C. Uher, T. Hogan, E.K. Polychroniadis, M.G. Kanatzidis, Science 303 (2004) 818.
[8] D. Bilc, S.D. Mahanti, E. Quarez, K.F. Hsu, R. Pcionek, M.G. Kanatzidis, Physical Review Letters 93 (2004).
[9] N. Chen, F. Gascoin, G.J. Snyder, E. Muller, G. Karpinski, C. Stiewe, Applied Physics Letters 87 (2005).
[10] H. Lin, E.S. Bozin, S.J.L. Billinge, E. Quarez, M.G. Kanatzidis, Physical Review B 72 (2005).
[11] E. Quarez, K.F. Hsu, R. Pcionek, N. Frangis, E.K. Polychroniadis, M.G. Kanatzidis, Journal of the American Chemical Society 127 (2005) 9177.
[12] D.I. Bilc, S.D. Mahanti, M.G. Kanatzidis, Physical Review B 74 (2006).
[13] H. Hazama, U. Mizutani, R. Asahi, Physical Review B 73 (2006).
[14] F.R. Drymiotis, T.B. Drye, Y.S. Wang, J. He, D. Rhodes, K. Modic, S. Cawthorne, Q.R. Zhang, Journal of Applied Physics 107 (2010).
[15] T.B. Massalski, H. Okamoto, ASM International, Binary Alloy Phase Diagrams, ASM International, Materials Park, Ohio, 1990.
[16] M. Ferhat, J. Nagao, Journal of Applied Physics 88 (2000) 813.
[17] M. Fujikane, K. Kurosaki, H. Muta, S. Yamanaka, Journal of Alloys and Compounds 393 (2005) 299.
[18] M. Fujikane, K. Kurosaki, H. Muta, S. Yamanaka, Journal of Alloys and Compounds 387 (2005) 297.
[19] J. Capps, F. Drymiotis, S. Lindsey, T.M. Tritt, Philosophical Magazine Letters 90 (2010) 677.
[20] F. Drymiotis, T. Drye, D. Rhodes, Q. Zhang, J.C. Lashey, Y. Wang, S. Cawthorne, B. Ma, S. Lindsey, T. Tritt, Journal of Physics-Condensed Matter 22 (2010).